Exploration of a $Ca_{1-x}(NaCe)_{x/2}Bi_4Ti_{3.98}(WNb)_{0.01}O_{15}$ ceramic intermediate phase by temperature-dependent spectroscopic ellipsometry and Raman scattering

Qiong Ding (丁穷), Liping Xu (徐丽萍), Jinzhong Zhang (张金中), Kai Jiang (姜凯), Zhigao Hu (胡志高), Zhiyong Zhou (周志勇), Xianlin Dong (董显林), and Junhao Chu (褚君浩)

Citation: Journal of Vacuum Science & Technology B **37**, 061211 (2019); doi: 10.1116/1.5118791
View online: https://doi.org/10.1116/1.5118791
View Table of Contents: https://avs.scitation.org/toc/jvb/37/6
Published by the American Vacuum Society

Exploration of a $Ca_{1-x}(NaCe)_{x/2}Bi_4Ti_{3.98}(WNb)_{0.01}O_{15}$ ceramic intermediate phase by temperature-dependent spectroscopic ellipsometry and Raman scattering

Qiong Ding (丁穷),[1] Liping Xu (徐丽萍),[1] Jinzhong Zhang (张金中),[1,a)] Kai Jiang (姜凯),[1] Zhigao Hu (胡志高),[1,2,3,b)] Zhiyong Zhou (周志勇),[4] Xianlin Dong (董显林),[4] and Junhao Chu (褚君浩)[1]

[1]*Technical Center for Multifunctional Magneto-Optical Spectroscopy (Shanghai), Department of Electronic Engineering, East China Normal University, Shanghai 200241, China*
[2]*Collaborative Innovation Center of Extreme Optics, Shanxi University, Taiyuan, Shanxi 030006, China*
[3]*Shanghai Institute of Intelligent Electronics & Systems, Fudan University, Shanghai 200433, China*
[4]*Key Laboratory of Inorganic Functional Materials and Devices, Shanghai Institute of Ceramics, Chinese Academy of Sciences, Shanghai 200050, China*

(Received 4 July 2019; accepted 21 October 2019; published 13 November 2019)

Different doping concentrations of $Ca_{1-x}(NaCe)_{x/2}Bi_4Ti_{3.98}(WNb)_{0.01}O_{15}$ ($x = 0$, 3%, 4%, 5%, and 6%) were prepared by a traditional solid state reaction method. The effects of doping on the crystal structure, dielectric constant, electronic transitions, and lattice dynamics of doped $CaBi_4Ti_4O_{15}$ were investigated by x-ray diffraction, temperature-dependent spectroscopic ellipsometry, and Raman scattering. The results showed that, when $x < 4\%$, the substitution of Na [$r_{Na} = 0.95$ Å with a coordination number (CN) = 6] is dominant, and the crystal structure symmetry is weakened. When $x > 4\%$, the substitution of Ce ($r_{Ce} = 1.01$ Å, CN = 6) is dominant, and the crystal structure symmetry begins to increase. As the doping concentration increases, the optical bandgap initially increases and then decreases, which is consistent with the evolution of the structural symmetry. Finally, evidence of the existence of an intermediate phase transformation of $CaBi_4Ti_4O_{15}$-based ceramics is extracted by analyzing the thermal evolution of the electronic transitions and Raman modes. Therefore, spectroscopic ellipsometry and Raman spectroscopy can be used to probe intermediate phase transformations in ferroelectrics. *Published by the AVS.* https://doi.org/10.1116/1.5118791

I. INTRODUCTION

Bismuth layer-structured ferroelectrics (BLSFs) have excellent ferroelectric properties such as good fatigue resistance and low leakage current and also a high Curie temperature, which make them suitable for high-temperature and high-frequency applications.[1] The BLSF is formed by the symbiotic arrangement of two-dimensional perovskite and $(Bi_2O_2)^{2+}$ layers according to certain rules, and it has the chemical formula $(Bi_2O_2)^{2+}(A_{n-1}B_nO_{3n+1})^{2-}$, where the constant $n = 1, 2, 3, 4, 5$ is the number of perovskite layers. The BLSF performance depends on the number of perovskite-like units, the BO_6 octahedral structure, and the chemical elements in positions A and B. In addition, material properties can be adjusted by selecting appropriate dopants at positions A and B, where the A site can be occupied by B^{3+}, Pb^{2+}, Ba^{2+}, Sr^{2+}, Ca^{2+}, Na^{+}, K^{+}, La^{3+}, Y^{3+}, U^{3+}, and Th^{4+} or by their corresponding composite ions. Furthermore, the B position is occupied by an ion suitable for octahedral coordination such as Co^{3+}, Cr^{3+}, Zr^{4+}, Ti^{4+}, Nb^{5+}, Ta^{5+}, W^{6+}, and Mo^{6+} or composite ions.[2] One typical BLSF is $CaBi_4Ti_4O_{15}$ (CBT), which belongs to the Aurivillius phase and has an n of 4, with Ca^{2+} and Bi^{3+} occupying the A position, and Ti^{4+} occupying the B position. The space group of CBT is $A2_1am$ (36)-orthorhombic at low temperatures, but it becomes the $I4/mmm$-cubic phase at about 1060 K. Its Curie temperature can reach 790 °C, which has broad application prospects and has made CBT one of the hotspots of research in recent years.[1,2] However, the application of CBT in high-temperature piezoelectrics is severely limited owing to its low piezoelectric activity (~7 pC/N).[3] It is, therefore, necessary to thoroughly explore the structural changes of these materials induced by doping to identify suitable ways to improve their performance and to achieve applications in high-temperature devices.

In dielectric materials used for applications, the dielectric function is an important physical parameter that can determine the refractive index and the extinction coefficient of the film/bulk materials. Spectroscopic ellipsometry is a powerful tool for studying the dielectric function of materials. Furthermore, the imaginary part of the dielectric function is related to the material's bandgap and electronic transition. Therefore, the variation of the dielectric function with temperature reflects the variation of electronic transition with temperature and can be used to explore the variation of the thermoelectric, ferroelectric, and dielectric properties of ferroelectric oxide materials. In addition, Raman spectroscopy is a nondestructive technique that can provide important information about the lattice vibrations and crystal symmetries of materials.

In this work, the physical mechanism of structural and performance changes of a CBT-based material as a function of doping and temperature was analyzed by the spectral method.

Note: This paper is part of the Conference Collection: 8th International Conference on Spectroscopic Ellipsometry 2019, ICSE.

[a)]Electronic mail: jzzhang@ee.ecnu.edu.cn
[b)]Electronic mail: zghu@ee.ecnu.edu.cn

In this experiment, Na^+ and Ce^{3+} ions were substituted for the A-site ion such that $Ca_{1-x}(NaCe)_{x/2}Bi_4Ti_{3.98}(WNb)_{0.01}O_{15}$ (CBT-NCx), where x is 0, 3%, 4%, 5%, and 6% (abbreviated as CBT-NC0, CBT-NC3, CBT-NC4, CBT-NC5, and CBT-NC6, respectively). The main work focused on the material's performance as a function of doping concentration and temperature as analyzed by condensed matter spectroscopy, and it provides theoretical support for developing CBT-based applications in the near future.

II. EXPERIMENTAL DETAILS

The CBT-NCx samples were prepared by a traditional solid state reaction method with $CaCO_3$, Bi_2O_3, TiO_2, Na_2CO_3, CeO_2, Nb_2O_5, and WO_3 as raw materials. Bi_2O_3 was added in an excess of 2% owing to the small amount of Bi volatilization during the process. The raw materials were mixed via ball milling with distilled water as the milling medium, and they were subsequently dried and then sintered at 940 °C for 3 h. The sintered powder was pulverized and dried and then pressed into a disk with a diameter of 13 mm and a thickness of about 1.5 mm under a pressure of 250 MPa. The formed wafer was sealed and sintered at 1200 °C for 2 h and then naturally cooled within a furnace. Finally, the samples were thinned, polished, coated with the gold paste, annealed at 800 °C for 10 min, and then naturally cooled to room temperature.

The crystalline structures of CBT-NCx ceramics can be studied by x-ray diffraction (XRD) with an Ni-filtered Cu $K\alpha$ radiation source (D/MAX-2550 V, Rigaku Co.). The ellipsometric measurements were investigated by near infrared–ultraviolet spectroscopic ellipsometry (V-VASE by J. A. Woollam Co., Inc.) for a photon energy range of 2.3–5.7 eV and a temperature range of 200–800 K. The spectral resolution was 5 nm and the incident angle was 70°. Furthermore, micro-Raman spectrometry (Jobin-Yvon LabRAM HR 800 UV) was used for temperature-dependent Raman scattering measurements in the range of 200–800 K using a 532 nm-wavelength He-Ne laser beam as the excitation source focused with a 50× microscope.

III. RESULTS AND DISCUSSION

Figure 1 shows the XRD patterns of the CBT-NCx ceramics measured at room temperature, where all diffraction peaks are identified using the standard diffraction spectrum of CBT (JCPDS: 52-1640). The diffraction peaks of the samples are consistent with the standard diffraction spectrum of CBT, belong to the orthomorphic space group $A2_1am$ (36), and exhibit no secondary phase, where the latter indicates that CBT-NCx ceramics have a single phase. The highest diffraction peak from the (119) plane confirms the rule that the highest diffraction peak of an Aurivillius material is from the $(112n+1)$ plane near $2\theta = 30.5°$.[4,5] For our samples, as x increases, the intensity of the (119)-plane diffraction peak initially decreases and then increases. This peak intensity variation can be explained by the fact that, when $x < 0.04$, the substitution of Na [Na ionic radius

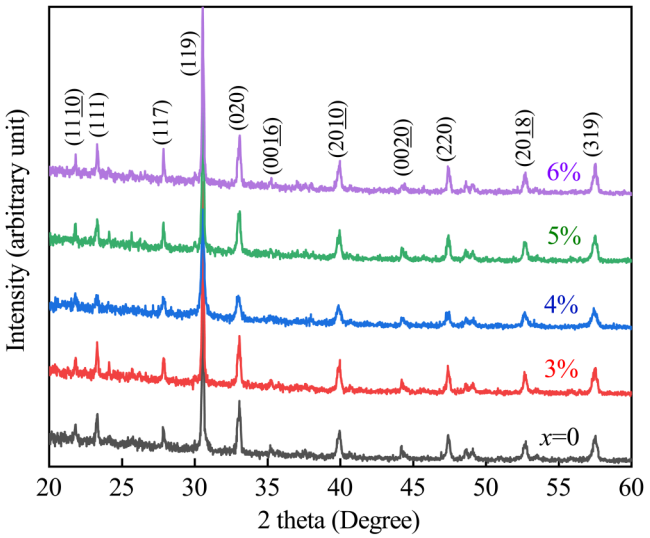

FIG. 1. XRD patterns of the CBT-NCx ceramics at room temperature.

$r_{Na} = 0.95$ Å, coordination number (CN)=6] is dominant; but when $x > 0.04$, the substitution of Ce (Ce ionic radius $r_{Ce} = 1.01$ Å, CN = 6) is dominant ($r_{Ca} = 0.99$ Å).[6,7] Because the ionic radius of Na is smaller than that of Ca, initially, the tolerance factor $t = (r_A + r_O)/\sqrt{2}(r_B + r_O)$ decreases when $x < 0.04$ and the symmetry of the crystal structure weakens. Furthermore, the ionic radius of Ce is larger than that of Ca, and thus the tolerance factor t increases when $x > 0.04$, and the symmetry of the crystal structure enhances.[8] With increasing concentrations of Na and Ce, the intensities of the (006), (008), (0010), and (0016) diffraction peaks also become stronger. This phenomenon indicates that a small amount of Na^+ and Ce^{3+} ion doping is conducive to the growth of the grain along the c axis and for increasing grain size, which is beneficial to reduce the anisotropy of ceramic grains. Owing to the requirement of electrical neutrality, A-position vacancies (i.e., Ca and Bi vacancies) are easily formed and result in lattice distortion, where the Ca vacancies contribute more to the distortion than Bi vacancies. During the high-temperature sintering, a large amount of bismuth volatilization occurs and thus a large number of Bi vacancies are formed, which limits the formation of Ca vacancies and results in a small degree of lattice distortion. Therefore, the lattice distortion mainly originates from the doping of the A site.

Spectroscopic ellipsometry is a technique for studying the optical properties of film/bulk materials using the polarization phenomenon of light. The test parameters Ψ and Δ are used to represent the change in intensity and phase of the polarized light, respectively, and the experimental parameters investigated by ellipsometry are the elements of the complex ratio $\rho = r_p/r_s = \tan\Psi e^{i\Delta}$, where r_p and r_s are the reflection coefficients of the parallel and vertical components, respectively. Considering the interface between the air and the sample, the dielectric function ε can be expressed as[9] $\varepsilon = \varepsilon_r + i\varepsilon_i = \sin^2\Phi[1 + \tan^2\Phi(1-\rho)^2/(1+\rho)^2]$, where Φ represents the angle of incidence; and ε_r and ε_i represent the real and imaginary parts of dielectric function, respectively.

In this work, the effect of element doping and temperature on the dielectric function of CBT-NC*x* ceramics was investigated by spectroscopic ellipsometry.

The experimental ellipsometric spectra of Ψ and Δ and their best Tauc-Lorentz model fitting are shown in Figs. 2(a) and 2(b) for the CBT-NC3 and CBT-NC6 ceramics, respectively, at room temperature. It can be seen that the experimental spectra can be fitted well with the Tauc-Lorentz function. Figure 2(c) shows the complex dielectric function components of CBT-NC*x* extracted from the experimental data, which suggests that the entire imaginary part from the CBT-NC*x* ceramics ε_i is 0 when the photon energy is less than 3.3 eV. ε_i denotes the material's absorption of photon energy, so it can be inferred that the CBT-NC*x* ceramic does not absorb photons whose energy is less than 3.3 eV. The value of the parameter ε_i increases with energy, which signifies that, when the photon energy exceeds the optical bandgap E_g of the material, electronic transitions appear from the valence band to the conduction band. The relationship between the Na, Ce concentrations and E_g was obtained [Fig. 2(d)], which reveals that the E_g initially increases and then decreases with increasing Na and Ce concentration. This result is consistent with the structural change of CBT-NC*x* with concentration as measured by the XRD technique. These trends are all caused by the lattice structure changes of the doped CBT. From the perspective of electronic transitions, the Bi-6s and O-2p orbital hybridization present in a BLSF forms its valence bands,[9] while the substitution of Na^+ and Ce^{3+} ions with different concentrations affects the structure of CBT-NC*x* and the optical bandgap E_g.

To investigate the effect of temperature on the electronic transitions of CBT-NC*x*, we performed a variable temperature ellipsometry experiment, as shown in Figs. 3(a)–3(d). From Fig. 3(b), the low energy region of the spectra shows that ε_r and ε_i of CBT-NC3 are about 5.3 and 0, respectively, which indicates that CBT-NC3 does not absorb in this energy

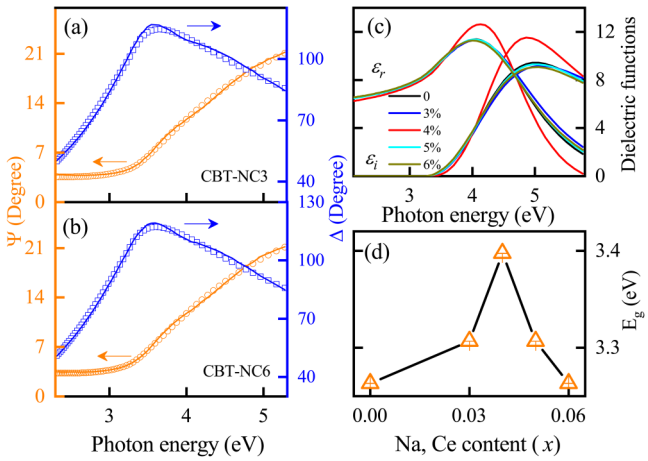

FIG. 2. (a) Experimental ellipsometric Ψ (left axis) and Δ (right axis) spectra (data points) and their best Tauc-Lorentz function fit (solid line) of (a) CBT-NC3 and (b) CBT-NC6 ceramics at room temperature. (c) The complex dielectric function components ε_r (real component) and ε_i (imaginary component) of CBT-NC*x* ceramics at room temperature. (d) The optical bandgap E_g as a function of the Na and Ce content.

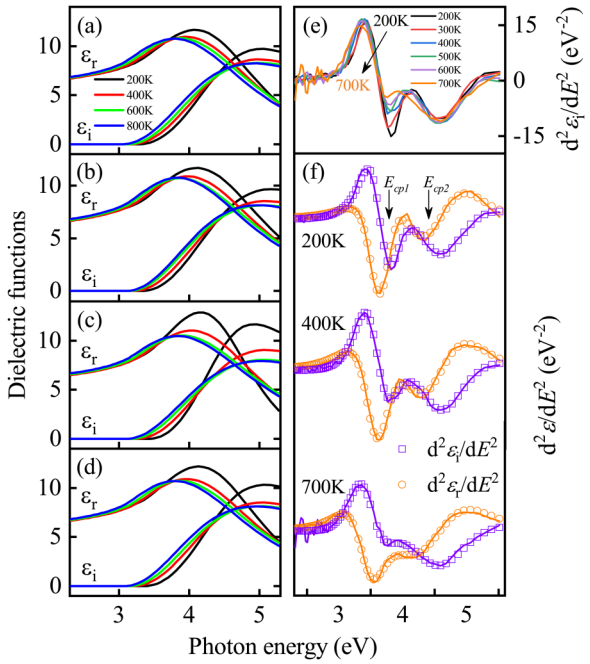

FIG. 3. Real and imaginary parts of the dielectric function for CBT-NC*x* ceramics with different temperature for (a) CBT-NC0, (b) CBT-NC3, (c) CBT-NC4, and (d) CBT-NC5. (e) The second partial derivative spectra for the imaginary part ($d^2\varepsilon_i/dE^2$) of the pseudo-dielectric functions for CBT-NC0 at various temperatures. (f) The second derivatives of the dielectric functions ($d^2\varepsilon/dE^2$) spectra (symbols) and the best-fitted spectra (solid lines) at 200, 400, and 700 K for CBT-NC0.

range. When the photon energy is greater than the bandgap, the electrons have enough energy to cross the bandgap. So, the material begins to absorb photon energy[10,11] and ε_i exhibits two absorption peaks at around 3.3 and 4.7 eV, as indicated by the arrow. These two absorptions (labeled E_{cp1} and E_{cp2}) are the two exciton absorption critical points. Using the value of the energy absorbed at ε_i, we can determine that the bandgap E_g decreases with increasing temperature, which is consistent with the fact that the semiconductor bandgap has a negative temperature coefficient.[12,13]

The variation of ε_r and ε_i for CBT-NC3 is the same as that of CBT-NC0 for the entire photon energy range, where the values of the real and imaginary parts of the dielectric function increase at lower energies and then decrease at higher energies with increasing temperature. The complex dielectric function of other CBT-NC*x* ceramics has a similar trend with increasing temperature.[14] Because the location of E_{cp1} and E_{cp2} is not clearly evident in Figs. 3(a)–3(d), we studied the second-order derivative $d^2\varepsilon/dE^2$ using the standard critical point (SCP) model,[15]

$$\frac{d^2\varepsilon}{dE^2} = \begin{cases} n(n-1)A_m e^{i\phi_m}(E - E_{cpm} + i\Gamma)^{n-2}, & n \neq 0, \\ A_m e^{i\phi_m}(E - E_{cpm} + i\Gamma_m)^{-2}, & n = 0, \end{cases}$$

where m denotes the oscillator number, and A_m, E_{cpm}, Γ_m, and ϕ_m are the amplitude, threshold energy, broadening, and phase angle, respectively. The index n indicates that the corresponding one-dimensional (1D), two-dimensional (2D), and three-dimensional (3D) critical points of the exciton

TABLE I. Parameters of the standard critical point model for CBT-NCx ceramics, whose values were extracted from the best-fit second derivatives of the complex dielectric functions.

Samples	$x = 0.00$			$x = 0.03$			$x = 0.04$			$x = 0.05$			$x = 0.06$		
T (K)	200	400	700	200	400	700	200	400	700	200	400	700	200	400	700
A_1	0.74	0.95	0.81	0.90	0.71	0.72	0.65	0.61	0.85	1.00	0.70	0.72	0.74	0.78	0.9
	(0.01)	(0.02)	(0.13)	(0.03)	(0.03)	(0.19)	(0.02)	(0.02)	(0.04)	(0.12)	(0.04)	(0.12)	(0.03)	(0.10)	(0.02)
ϕ_1 (deg)	20.75	20.27	19.78	20.87	20.24	19.64	20.99	20.44	20.26	21.25	20.24	19.77	20.73	20.43	19.92
	(0.05)	(0.04)	(0.06)	(0.03)	(0.02)	(0.05)	(0.01)	(0.03)	(0.09)	(0.04)	(0.10)	(0.09)	(0.06)	(0.00)	(0.06)
E_{cp1} (eV)	3.67	3.58	3.45	3.69	3.55	3.41	3.65	3.56	3.53	3.73	3.58	3.42	3.66	3.59	3.45
	(0.01)	(0.00)	(0.01)	(0.01)	(0.00)	(0.01)	(0.10)	(0.00)	(0.02)	(0.01)	(0.01)	(0.01)	(0.02)	(0.04)	(0.01)
Γ_1 (eV)	0.42	0.48	0.50	0.45	0.43	0.48	0.42	0.42	0.50	0.46	0.42	0.48	0.41	0.44	0.51
	(0.00)	(0.01)	(0.02)	(0.00)	(0.01)	(0.04)	(0.00)	(0.00)	(0.01)	(0.01)	(0.01)	(0.04)	(0.01)	(0.02)	(0.01)
A_2	4.48	4.62	7.38	3.64	4.72	6.30	4.39	4.84	5.34	4.14	5.20	6.74	4.54	4.96	5.64
	(0.14)	(0.23)	(0.52)	(0.06)	(0.40)	(1.54)	(0.06)	(0.33)	(0.14)	(0.18)	(0.06)	(0.37)	(0.72)	(0.1)	(0.20)
ϕ_2 (deg)	15.56	21.66	8.99	9.03	9.32	8.96	9.79	9.33	8.79	8.82	9.22	8.86	9.30	9.19	15.19
	(0.09)	(0.04)	(0.16)	(0.04)	(0.07)	(0.14)	(0.03)	(0.04)	(0.07)	(0.02)	(0.19)	(0.03)	(0.13)	(0.04)	(0.07)
E_{cp2} (eV)	4.56	4.54	4.44	4.50	4.56	4.40	4.61	4.51	4.37	4.42	4.55	4.37	4.57	4.51	4.37
	(0.03)	(0.01)	(0.06)	(0.01)	(0.03)	(0.04)	(0.01)	(0.02)	(0.01)	(0.02)	(0.07)	(0.02)	(0.03)	(0.01)	(0.02)
Γ_2 (eV)	0.92	0.93	1.10	0.84	0.97	1.06	1.01	1.00	1.01	0.86	0.97	1.07	0.91	0.97	1.01
	(0.01)	(0.02)	(0.05)	(0.01)	(0.02)	(0.08)	(0.01)	(0.01)	(0.01)	(0.01)	(0.02)	(0.01)	(0.06)	(0.02)	(0.02)

correspond to the values of −0.5, 0, and 0.5, respectively.[16] Figure 3(e) shows the second partial derivative spectra of the imaginary part of the dielectric constant for CBT-NC0 at various temperatures. The two valleys present in each spectrum correspond exactly to the electronic transitions of E_{cp1} and E_{cp2}. Moreover, a redshift phenomenon of these valleys is observed upon heating, which is mainly caused by the thermal expansion of the crystal lattice.[17,18] To derive the exact location of E_{cp1} and E_{cp2}, we need to fit the second derivative of the real and imaginary parts of the dielectric constant using the SCP model,[19,20] and the fitting results are shown in Fig. 3(f). From the fitting data, we extracted the values of A_m, E_m, Γ_m, and ϕ_m of the CBT-NCx ceramics at 200, 400, and 700 K, which are listed in Table I.

Figures 4(a)–4(d) show the values of E_{cp1} and E_{cp2} of CBT-NC0 and CBT-NC4 as a function of temperature. With increasing temperature, the electronic transitions E_{cp1} and E_{cp2} exhibit a significant redshift, and the slope of the line through the data changes at about 500 and 540 K for CBT-NC0 and CBT-NC4, respectively. For BLSFs, E_{cp1} is mainly affected by the p orbital of the ions at the A site and the p orbital of the O anion, while E_{cp2} is related to the d orbital of the ions at the B site.[21] Because the paraelectric phase is a completely symmetric cubic structure, as the temperature increases, the off-center B-site cation slowly moves to the center of the BO_6 octahedron during the transition from the ferroelectric phase to the paraelectric phase.[22,23] The movement of the B-site cation affects the orbital hybridization of atoms in the BO_6 octahedron, which causes E_{cp1} and E_{cp2} to undergo the same trends. In addition, the abnormal changes in the electronic transition energy E_{cp1} and E_{cp2} between the bands indicate a change in the crystalline structure, and it is further considered that an intermediate phase is generated.

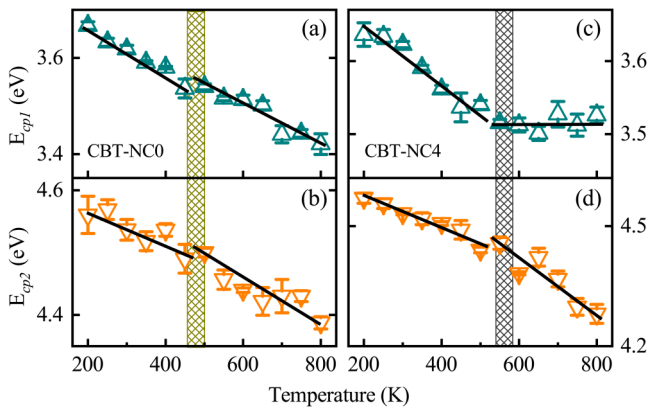

FIG. 4. Thermal evolution of the values of two exciton absorption critical points (a) and (c) E_{cp1} and (b) and (d) E_{cp2} for (a) and (b) CBT-NC0 and (c) and (d) CBT-NC4. The solid lines are a guide for the eye to emphasize the various trends.

The thermal evolution of the CBT-NCx ceramics was investigated by temperature-dependent Raman spectroscopy, where Figs. 5(a) and 5(b), respectively, show the Raman spectra of CBT-NC0 and CBT-NC4 ceramics recorded at various temperatures. The Raman-active modes around 55, 230, and 550 cm^{-1} are related to the vibrations of the B-site ions, the Bi–O bond in the $(Bi_2O_2)^{2+}$ layer,[24] and equatorial oxygen atoms in the Ti-O plane, respectively.[25] Therefore, we mainly discuss the variations of frequency, broadening, and intensity of these four first-order Raman modes as a function of temperature. In Fig. 5, the Raman spectrum at 200 K is taken as an example to show the Lorentz function fitting condition used herein, where the experimental and fitted spectra are clearly in good agreement. The Raman peaks in the range of 250–400 cm^{-1} gradually reduce in intensity with increasing temperature, and broadening tends to go up as the temperature increases, which reflects the reduction of the internal structure distortion and the improvement of symmetry. The phonon mode around 590 cm^{-1}

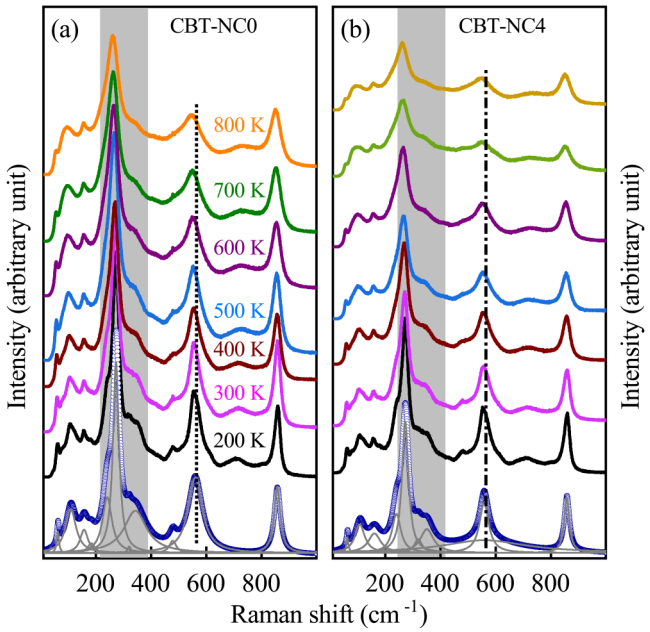

FIG. 5. Raman spectra of (a) CBT-NC0 and (b) CBT-NC4 ceramics at various temperatures after correcting for the thermal population factor and the corresponding multi-Lorentz peak fitting at 200 K. For clarity, each spectrum is shifted in intensity.

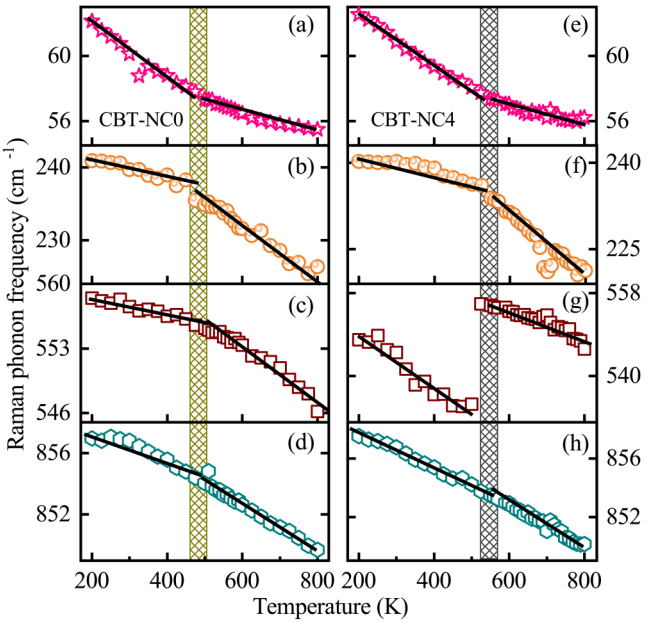

FIG. 6. Frequency trends as a function of temperature of some typical Raman-active modes for (a)–(d) CBT-NC0 and (e)–(h) CBT-NC4 ceramics. The solid lines are a guide for the eye to emphasize the various trends, and the shaded areas indicate the boundary between adjacent phases.

(near the vertical dashed line in Fig. 5) has a significant redshift with increasing temperature because of the lattice expansion and the interaction between the anharmonic phonons and the phonons.[26]

To investigate the temperature dependence of Raman phonons, all experimental spectra were fitted by the multi-Lorentz oscillator model. We note that all spectra were corrected using the Bose–Einstein temperature factor before fitting to eliminate the effect of the Bose–Einstein population factor on the scattering intensity.[27,28] By fitting the Raman spectra, the frequency of some temperature-dependent phonons can be extracted, as shown in Fig. 6. These plots of the four phonon modes suggest that the mode frequencies exhibit a significant redshift with temperature owing to the thermal expansion of the crystal lattice and the anharmonic phonon-phonon interaction.[29] However, the Raman peaks from CBT-NC0 and CBT-NC4 exhibit an abnormal trend at around 500 and 550 K, respectively, that cannot be explained only by the thermal expansion theory. This abnormal Raman phonon mode change with temperature is likely caused by the occurrence of a phase transition, where the CBT-ceramic samples undergo an intermediate phase transformation in the temperature range of 200–800 K. It can be seen in Fig. 6 that the transition temperatures of CBT-NC0 and CBT-NC4 are about 500 and 550 K, respectively. These results are in complete agreement with those derived from temperature-dependent ellipsometric spectra, and a similar phenomenon can be found in other components. For example, the variation trends of the Raman phonons during the heating process of $SrBi_2Ta_2O_9$ and Bi_3TiNbO_9 materials also indicate that there is an intermediate phase between the ferroelectric phase $A2_1am$ and paraelectric phase $I4/mmm$.[30] Therefore, it can be concluded that the CBT ceramics possess an intermediate phase before the ferroelectric-paraelectric transition.

Combining the results of the evolution of the temperature-dependent electronic transitions and of the Raman-active modes, evidence of an intermediate phase transition of the CBT-NCx ceramics is found, as shown in Fig. 7. The intermediate phase transformations of CBT-NC0, CBT-NC3, CBT-NC4, CBT-NC5, and CBT-NC6 ceramics occur at

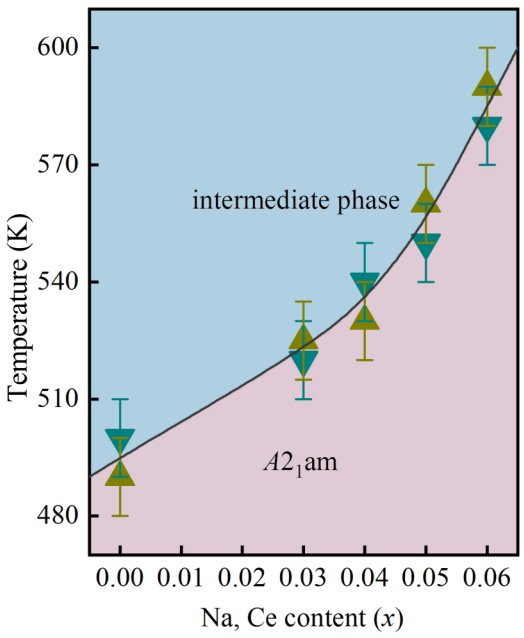

FIG. 7. Phase diagram of CBT-NCx ceramics with different Na and Ce contents. The phase transformation temperatures in the present work show the spectroscopic ellipsometry results (▲) and the Raman results (▼).

approximately 500, 520, 540, 550, and 580 K, respectively. This result reveals that phase transition temperature increases as the doping concentration of CBT-NCx is increased. The obtained evidence of an intermediate phase is significant for applications of this material in high-temperature devices. Therefore, phase transformations of ferroelectrics can be determined based on the temperature-dependent optical bandgap, optical constants, frequency, broadening, and intensity of Raman-active modes of a material.

IV. CONCLUSIONS

In summary, CBT-NCx ceramics with various doping concentrations belong to the orthomorphic space group $A2_1am$ (36) at room temperature, while the symmetry of the crystal structure is slightly disturbed owing to the different radii of the doping ions. The optical constants and electronic transitions are extracted by fitting ellipsometric spectra obtained at various temperatures. The results indicate that the CBT-NCx ceramics have an intermediate phase transition at around 500, 520, 540, 550, and 580 K for the CBT-NC0, CBT-NC3, CBT-NC4, CBT-NC5, and CBT-NC6 samples, respectively. These results are confirmed by the evolution of the temperature-dependent positions, intensity, and broadening of the first-order Raman-active modes near 56, 230, 550, and 855 cm^{-1}. Therefore, one can probe phase transformations of ferroelectric ceramics based on the temperature-dependent ellipsometric and Raman spectra.

ACKNOWLEDGMENTS

This work was financially supported by the National Key R&D Program of China (Grant Nos. 2017YFA0303403 and 2018YFB0406500), the National Natural Science Foundation of China (NNSFC) (Grant Nos. 61674057 and 91833303), the Projects of Science and Technology Commission of Shanghai Municipality (Grant Nos. 18JC1412400, 18YF1407200, and 18YF1407000), and the Program for Professor of Special Appointment (Eastern Scholar) at Shanghai Institutions of Higher Learning.

[1]T. Takenaka and H. Nagata, J. Eur. Ceram. Soc. **25**, 2693 (2005).
[2]N. Yasuda, T. Banno, and K. Fujita, J. Phys. Condens. Matter **18**, 7659 (2006).
[3]C. M. Wang, J. F. Wang, and L. M. Zheng, Mater. Sci. Eng. B **17**, 79 (2010).
[4]C. M. Wang, J. F. Wang, S. Zhang, and T. R. Shrout, J. Appl. Phys. **3**, 094110 (2009).
[5]P. Y. Fang, P. Liu, Z. Z. Xi, W. Long, and X. J. Li, Mater. Sci. Eng. B **186**, 21 (2014).
[6]H. X. Yan, Z. Zhang, and W. M. Zhu, Mater. Res. Bull. **39**, 1237 (2004).
[7]R. D. Shannon, Acta Cryst. A **32**, 751 (1976).
[8]D. F. Peng, H. Zou, and C. N. Xu, Ferroelectrics **450**, 113 (2013).
[9]A. B. Djurišić, Y. Chan, and E. H. Li, Mater. Sci. Eng. R **38**, 237 (2002).
[10]J. Z. Zhang *et al.*, Phys. Rev. B **91**, 085201 (2015).
[11]X. Zhang, H. Yan, and M. J. Reece, J. Am. Ceram. Soc. **91**, 2928 (2008).
[12]H. X. Yan, H. T. Zhang, M. J. Reece, and X. L. Dong, Appl. Phys. Lett. **87**, 082911 (2005).
[13]D. Faltermeier, B. Gompf, M. Dressel, A. K. Tripathi, and J. Pflaum, Phys. Rev. B **74**, 125416 (2006).
[14]Q. L. Deng, J. Z. Zhang, T. Huang, L. P. Xu, K. Jiang, Y. W. Li, Z. G. Hu, and J. H. Chu, J. Mater. Chem. C **3**, 8225 (2015).
[15]P. Lautenschlager, M. Garriga, L. Viña, and M. Cardona, Phys. Rev. B **36**, 4821 (1987).
[16]J. Z. Zhang, K. Jiang, Z. Y. Zhou, Z. G. Hu, G. S. Wang, X. L. Dong, and J. H. Chu, J. Am. Ceram. Soc. **99**, 3610 (2016).
[17]K. Shi, L. Peng, M. J. Li, Z. Y. Zhou, K. Jiang, J. Z. Zhang, Z. G. Hu, X. L. Dong, and J. H. Chu, J. Alloys Compd. **653**, 168 (2015).
[18]G. E. Jellison and F. A. Modine, Appl. Phys. Lett. **69**, 371 (1996); G. E. Jellison and F. A. Modine, Appl. Phys. Lett. **69**, 2137 (1996).
[19]D. A. G. Bruggeman, Ann. Phys. (Leipzig) **416**, 636 (1935).
[20]S. G. Choi, H. T. Yi, S. W. Cheong, J. N. Hilfiker, R. France, and A. G. Norman, Phys. Rev. B **83**, 100101 (2011).
[21]Q. Q. Li, J. Y. Wang, M. J. Li, S. Guo, J. Z. Zhang, Z. G. Hu, Z. Y. Zhou, G. S. Wang, X. L. Dong, and J. H. Chu, Phys. Rev. B **96**, 024101 (2017).
[22]E. C. Subbarao, J. Phys. Chem. Solids **23**, 665 (1962).
[23]S. P. Pavunny, A. Kumar, and R. S. Katiyar, J. Appl. Phys. **107**, 013522 (2010).
[24]K. R. Whittle, N. C. Hyatt, and I. M. Reaney, Chem. Mater. **20**, 6427 (2008).
[25]C. B. Long, H. Q. Fan, and P. R. Ren, Inorg. Chem. **52**, 5045 (2013).
[26]E. Buixaderas, I. Gregora, J. Hlinka, J. Dec, and T. Lukasiewicz, Phase Transit. **86**, 217 (2013).
[27]A. Kiraci and H. Yurtseven, Ferroelectrics **450**, 93 (2013).
[28]M. R. Shen, G. G. Siu, Z. K. Xu, and W. W. Cao, Appl. Phys. Lett. **86**, 252903 (2005).
[29]H. C. Gupta, Archana, and V. Luthra, Vib. Spectrosc. **56**, 235 (2011).
[30]H. C. Gupta, Archana, and V. Luthra, J. Mol. Struct. **984**, 204 (2010).